Design and test of a compact compliant gripper using the Scott-Russell mechanism

Jiaxiang Zhu and Guangbo Hao *

School of Engineering-Electrical and Electronic Engineering, University College Cork, T12 K8AF Cork, Ireland

* Corresponding author: G.Hao@ucc.ie

Abstract:

This paper presents the design, modelling, fabrication, and test of a monolithic compliant gripper for micro-manipulation applications. A compact compliant mechanism that enables in-principle straight-line parallel jaw motion is obtained, by combining the Scott-Russell mechanism and the parallelogram mechanism. The Right-Circular Corner-Filleted (RCCF) flexure hinge is adopted to achieve a large displacement of lumped-compliance joints. A pseudo-rigid-body model (PRBM) method with the help of the virtual work principle is performed to obtain parametric analytical models including the amplification coefficient and kinetostatics. Finite element analysis (FEA) is conducted to validate the analytical model and capture adverse parasitic motions of jaws. A monolithic prototype was fabricated, the test results of which show satisfactory performances.

Keywords: compliant gripper; micro-manipulation; large displacement; straight-line motion; compact configuration

1. Introduction

The wide use of compliant mechanisms in precision systems is increasingly recognized in academia and industry due to their merits such as no backlash, no friction, and reduced part count [1]. One of their applications is in a micro-manipulation system where a compliant gripper is required to handle materials. A compliant gripper for micro-manipulation may be commissioned to assemble micro-parts [2] or operate microsurgery [3]. Therefore, a highly effective compliant gripper is desired to grip micro-objects with various sizes and different shapes without causing their damages [4]. From observing various compliant grippers reported in the literature, it is shown that researchers mainly focus on three aspects in the design of micro-grippers, namely novel actuation systems [5-7], novel mechanisms/structures [8-10] and new microfabrication techniques [11-13]. This paper focuses on the design of a novel gripper mechanism.

There are various issues inherited from the design of compliant gripper mechanisms. For instance, the basic parallelogram mechanism, which is commonly adopted by researchers [14-16] to generate a parallel gripping mode, has a relatively large parasitic motion (translation/rotation) worsening the performance of the gripper [17-19]. To mitigate this problem, a compliant mechanism with straight-line motion of its jaws can be pursued. Straight-line mechanisms such as Hoeken's linkage [20] and Scott-Russell mechanism [21] have been used to generate a straight-line motion. The Watt's linkage and the Chebyshev's linkage can also produce a straight-line motion, but their crossed-link structures constrain their applications [22]. The above straight-line mechanisms alone can generate a straight-line motion of a specified point but not produce a straight-line parallel jaw trajectory. Therefore, they have to be used in combining with other guiding mechanisms, which often cause complex and bulky designs [19-21]. This paper aims to address this issue by proposing a simple and compact compliant gripper.

Another challenge to design an effective gripper is how to achieve large displacement of jaws to satisfy the need in gripping objects with a broad range of sizes. Corner-filleted rectangular and right circular flexure hinges are two types of commonly used revolute (R) joints to design the gripper [23,24], while each of the designs has inherited limitations. The corner-filleted rectangular hinge can generate large motion range under elastic deformation, but it has an unwanted large drift of rotation

center. In contrast, the right circular hinge can produce a precise rotational motion, but the motion range is smaller than the rectangular one. By combining the advantages of these two joints, Chen et al. developed a novel flexure hinge named Right-Circular Corner-Filleted (RCCF) flexure hinge, which is able to produce relatively large motion with improved rotation precision [25]. This type of flexure hinge is to be embodied in this paper for the gripper design.

There are several well-known methodologies to model kinetostatics of compliant grippers, such as pseudo-rigid-body model (PRBM), finite element analysis (FEA) method and topology optimization. PRBM method means that the emerging analysis method for rigid linkage mechanisms can be used to study the performances of the corresponding compliant mechanisms [1,26,27]. The principle of topology optimization is to divide the structure into several sub-regions, which will be analyzed and interpreted, so that some redundant sections are eliminated according to specific optimization criteria [28,29].

The rest of this paper is organized as follows: Section 2 discusses the design and analysis of the compliant gripper. The results obtained in Section 2 are validated in section 3 by conducting FEA and experimental tests. Comparisons of results are illustrated in Section 4. Finally, the conclusion and future work are presented in Section 5.

2. Mechanism design and modeling

2.1. Design of a compliant gripper

To design the desired compliant gripper, a novel straight-line parallel jaw mechanism is first developed based on the Scott-Russell mechanism (Fig. 1). The Scott-Russell mechanism can be explained as an extension of slider-crank mechanism. It can not only generate a large-range exact straight-line motion for an output point but also be easily integrated with other mechanisms to enable a straight-line motion for an output rigid body (i.e. jaw) [30]. In this paper, a parallelogram mechanism is used to combine the original Scott-Russell mechanism as shown in Fig.1. Compared to other Scott-Russel based grippers [21,31], the present design is much simpler and more compact. This novel straight-line parallel jaw mechanism will be used to account for the kinematic model of the compliant gripper.

Based on the PRBM, the rigid-body mechanism will be correspondingly transformed into a monolithic compliant gripper by replacing the rigid kinematic joints with equivalent flexure hinges as presented in Fig.2. The novel compliant gripper mainly consists of rigid elements, identical RCCF flexure hinges, and a pair of double parallelogram mechanisms. The double parallelogram mechanism in the middle is adopted to act as the prismatic (P) joint, which can ensure a large linear input motion and stabilize the overall structure. To satisfy the design specifications, the mechanical structure is obtained by considerable modifications with the help of FEA. A symmetrical structure is presented to enable the identical movement of both jaws, thus reducing the traveling time. The

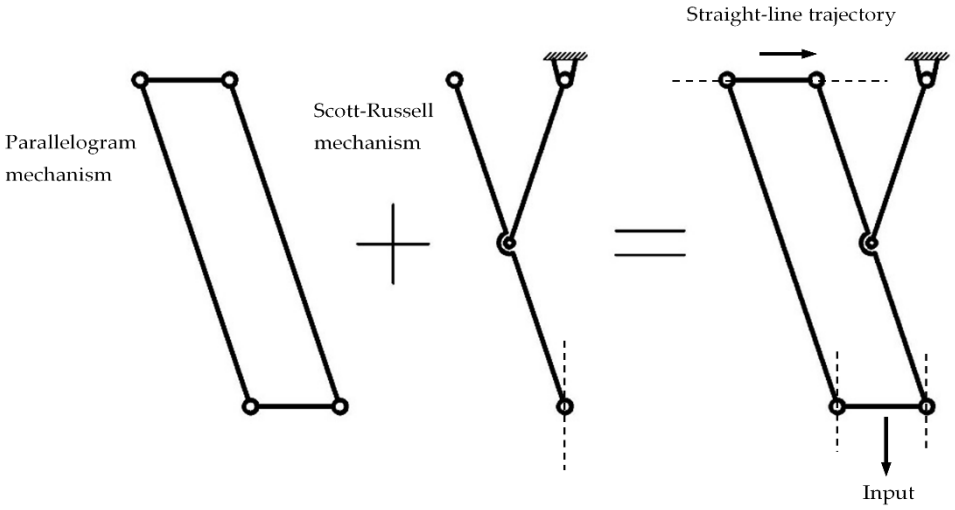

Figure 1 The novel straight-line parallel jaw mechanism

straight-line parallel jaw motion is achieved by the elastic deformation of the flexure hinges and the kinematic performance of the gripper is evaluated by the PRBM with the help of FEA.

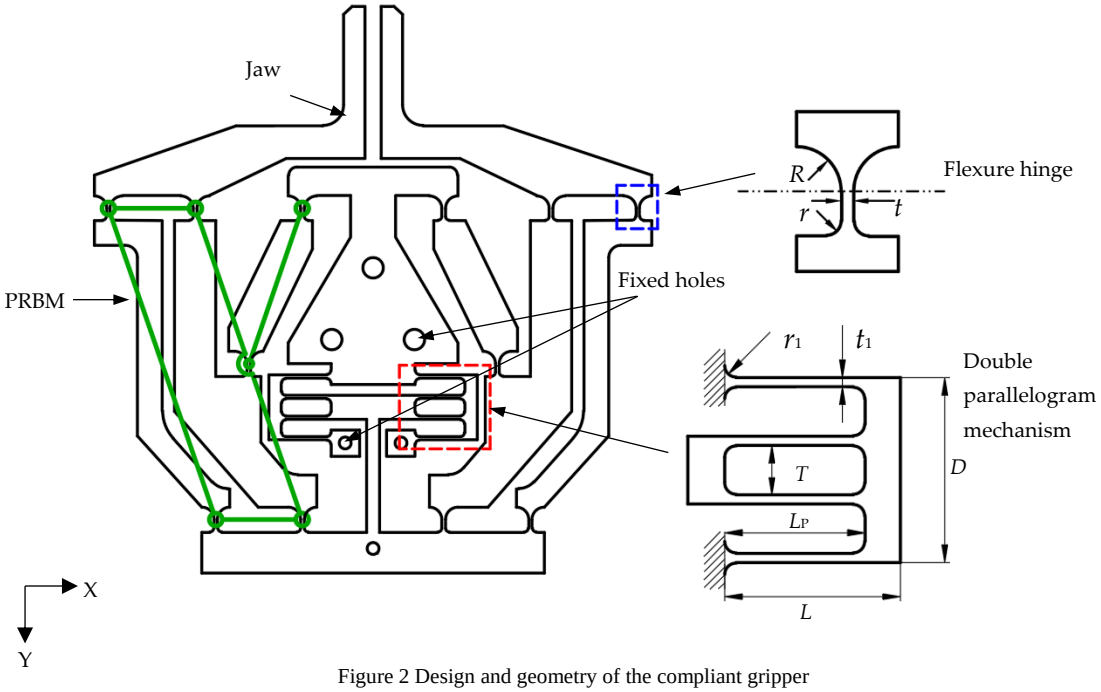

Figure 2 Design and geometry of the compliant gripper

2.2. *Kinematic model*

By implementing the PRBM, the motion of the gripper can be parametrically expressed by analyzing the kinematic model of the Scott-Russell mechanism, under the assumption that the elastic deformations in the gripper only occur in the compliant members/hinges and that the rest are rigid. Figure 3 labels all geometrical parameters, input displacement, output displacement, P joint and R joints of the left half rigid-body mechanism, which will be used to derive the kinematic model as follows. Let x_{out} be the (output) displacement of each jaw, and y_{in} be the (input) displacement of the P joint. In Fig. 3, α_0, d_{10} and d_{20} are the initial values of α, d_1 and d_2, respectively, in the configuration as fabricated.

The use of the right triangle relationship yields

$$d_{10}{}^2 + d_{20}{}^2 = d_1{}^2 + d_2{}^2 \tag{1a}$$

$$d_{20} = \sqrt{(2d_0)^2 - d_{10}{}^2} \tag{1b}$$

Given an input y_{in} along Y direction as shown in Fig.3, the jaw moves along the X direction (x_{out}). Based on Eq. (1a), the relation between y_{in} and x_{out} can be written as:

$$d_{10}{}^2 + d_{20}{}^2 = (d_{10} + y_{\text{in}})^2 + (d_{20} - x_{\text{out}})^2 \tag{2}$$

By solving Eq. (2), we can obtain the output displacement in term of the input displacement:

$$x_{\text{out}} = d_{20} - \sqrt{d_{20}{}^2 - 2d_{10}y_{\text{in}} - y_{\text{in}}{}^2} \tag{3}$$

Equation (3) shows a very simple kinematics of this gripper between the input and output.

The transmission of forces and displacements is achieved by the straight-line mechanism, which not only provides desired translational displacement of the jaw but also performs as an amplification mechanism. Using Eq. (3), the ratio between the output displacement and the input displacement can be obtained:

$$\left|\frac{x_{\text{out}}}{y_{in}}\right| = \left|\frac{d_{20} - \sqrt{d_{20}{}^2 - 2d_{10}y_{\text{in}} - y_{\text{in}}{}^2}}{y_{in}}\right| \tag{4}$$

It can be seen from Eq. (4) that the relationship between y_{in} and x_{out} is nonlinear. If input displacement is small enough, we can obtain:

$$|\frac{x_{\text{out}}}{y_{\text{in}}}| \cong \frac{d_{10}}{d_{20}} = cot\alpha_0 \tag{5}$$

where $cot\alpha_0$ is the simplified amplification factor of this gripper. It can be learned from Eq. (5) that the amplification ratio of the Scott-Russell mechanism is dominantly controlled by the initial angle α_0. Under a very small displacement range, the Scott-Russell mechanism can be seen as a mechanism with a constant amplification factor [32].

Let θ_{R} be the rotational angle of the flexure hinge R4, based on the basic geometric relationship, we can have

$$\theta_{\text{R}} = \alpha_0 - \alpha = \alpha_0 - arccos\left(\frac{d_{10} + y_{\text{in}}}{2d_0}\right) \tag{6}$$

where θ_{R} is also the rotational angle of hinge R2, R4, R5 or R6, and half the rotational angle of hinge R3.

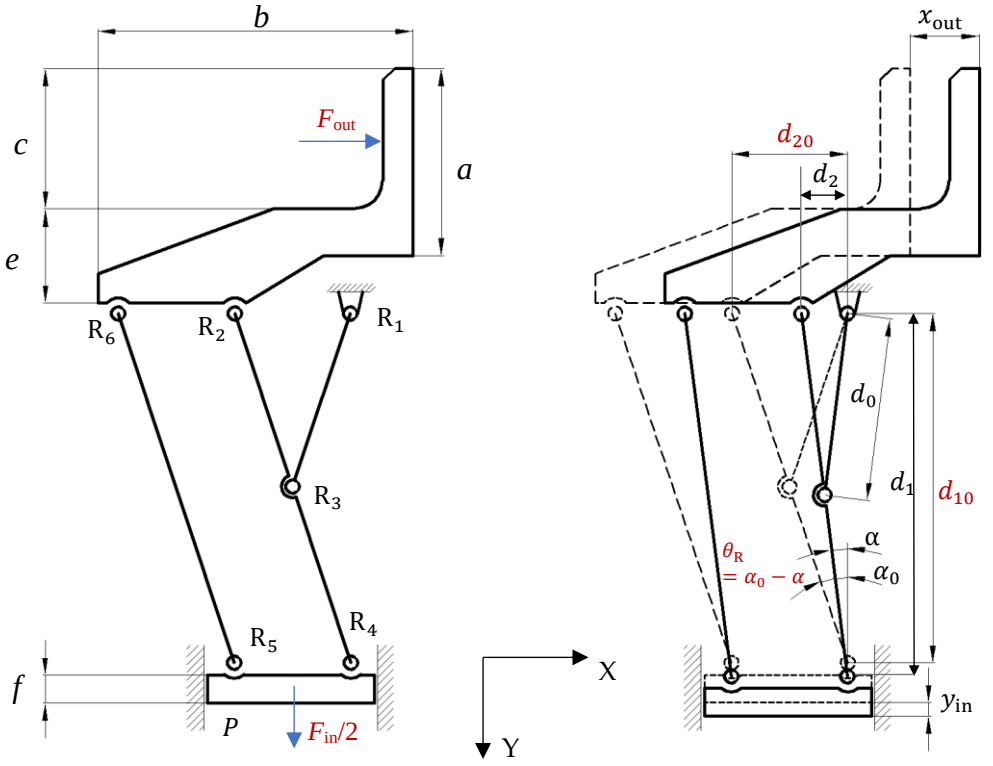

Figure 3 Kinematic model of half of compliant gripper (dotted line denoting the initial position)

2.3. *Kinetostatic model*

In this section, the kinetostatic model of the compliant gripper is to be derived step by step under the same assumption as provided in Sec. 2.2. The rotational stiffness of the RCCF hinge can be firstly obtained from Ref. [20] as below:

$$K_{\text{R}} = 1/[\frac{12}{Eh}\left(\frac{\gamma_1}{R^2} + \frac{R-r}{t^3} + \frac{\gamma_2}{r^2}\right)] \tag{7}$$

where

$$\gamma_1 = \frac{s_1^3(6s_1^2 + 4s_1 + 1)}{(2s_1 + 1)(4s_1 + 1)^2} + \frac{6s_1^4(2s_1 + 1)}{(4s_1 + 1)^{2.5}} arctg\sqrt{4s_1 + 1}$$

$$\gamma_2 = \frac{s_2^3(6s_2^2 + 4s_2 + 1)}{(2s_2 + 1)(4s_2 + 1)^2} + \frac{6s_2^4(2s_2 + 1)}{(4s_2 + 1)^{2.5}} arctg\sqrt{4s_2 + 1}$$

$$s_1 = {}^{R}/_{t}$$
$$s_2 = {}^{r}/_{t}$$

K_R is the stiffness of the RCCF hinge. h is the height of the hinge, which is also the out of plane thickness of the gripper. R, r, and t are defined in Fig. 2. E is the Young's modulus of the material. To simplify the expression of Eq. (7), the intermediate parameters, γ_1, γ_2, s_1 and s_2, are applied. The other symbols are explained in Fig. 2.

The linear stiffness of each P joint (the double parallelogram mechanisms) can then be obtained [33,34]:

$$K_{\mathrm{P}} = \frac{12EI}{L_{\mathrm{P}}^3} \tag{8}$$

where $I = ht_1^3/12$ is the area moment of inertia of a rectangular beam in the P joint. L_{P} is the length of the beam. t_1 is the thickness of the beam in the P joint. Note that the small fillets in the double parallelogram mechanism are not accommodated into the calculation of the stiffness.

Based on the virtual work principle [22], the relationship between the input force and input displacement can be derived for the compliant gripper. When the gripper is at a deformed position, the whole gripper system stores potential energy because of the bending of the flexure beams.

The total potential energy can be denoted:

$$\mathrm{U} = 2 \times \left[5 \times \left(\frac{1}{2}K_{\mathrm{R}}\theta_{\mathrm{R}}^2\right) + \frac{1}{2}K_R(2\theta_{\mathrm{R}})^2\right] + 2 \times \frac{1}{2}K_{\mathrm{P}}\mathrm{y}_{\mathrm{in}}^2 = 9K_R{\theta_{\mathrm{R}}}^2 + K_{\mathrm{P}}\mathrm{y}_{\mathrm{in}}^2 \tag{9}$$

The balance between the net virtual work by external forces and the gain of virtual energy leads to

$$F_{\mathrm{in}}\mathrm{d}y_{\mathrm{in}} + 2F_{\mathrm{out}}\mathrm{d}x_{\mathrm{out}} = \mathrm{d}U \tag{10a}$$

Equation (10a) with the help of Eqs. (3), (6), (9) can be rewritten as

$$F_{\mathrm{in}} = \frac{\mathrm{d}U}{\mathrm{d}y_{\mathrm{in}}} - 2F_{out}\frac{\mathrm{d}x_{\mathrm{out}}}{\mathrm{d}y_{\mathrm{in}}}$$

$$= 2 \times K_{\mathrm{P}}y_{\mathrm{in}} + 18K_{\mathrm{R}}\frac{\alpha_0 - \arccos(\frac{d_{10} + y_{\mathrm{in}}}{2d_0})}{\sqrt{4d_0^2 - (d_{10} + y_{\mathrm{in}})^2}} + 2F_{out}\frac{(d_{10} + y_{\mathrm{in}})}{\sqrt{4d_0^2 - (d_{10} + y_{\mathrm{in}})^2}} \tag{10b}$$

where F_{in} and F_{out} are the input force exerted on the gripper's bottom and reaction force exerted on the jaw, respectively. All those new symbols used in kinetostatic modelling in this section are presented in Table 1. Note that all the geometrical parameters used in Sec. 2.2 are labelled in Fig. 3 but not included in Table 1.

Equation (10b) build the relationship between the external forces and input displacement. If the gripper is applied to manipulate macro objects, which requires strong gripping force, the reaction force (i.e. F_{out} is minus) acting on the gripper jaw is nontrivial. However, the gripper presented in this paper is intended for gripping micro-objects like cells and tissues, so the reaction force exerted on the jaw can be trivial, which is to be neglected in FEA and experimental test.

Table 1: Parameters used in kinetostatics

Symbols	Definition
K_R	rotational stiffness of the RCCF hinge
K_{P}	linear stiffness of each P joint
E	elastic modulus of the material
I	area moment of inertia of the beam in the P joint
h	out of plane thickness of the gripper
t_1	thickness of the beam in the P joint
L_{p}	beam length in the P joint
r_1	beam fillet radius in the P joint
R	arc radius in the RCCF hinge
r	fillet radius in the RCCF hinge
t	minimum thickness of the RCCF hinge
F_{in}	input force of the gripper
F_{out}	reaction force on the jaw
U	total potential energy
$\gamma_1,\ \gamma_2,\ s_1,\ s_2$	intermediate parameters used in deriving K_R

3. FEA and testing

3.1. Parameter selection and simulation

We use Comsol 5.0 (COMSOL Inc., Stockholm, Sweden) to verify the present analytical models as well as analyse other performances such as the parasitic motion of two jaws that the analytical models cannot capture. A gripper design with geometrical parameters as shown in Table. 2 is selected as a case study. Those parameters are determined based on a number of reasons, some of which will be elaborated as follows.

To facilitate the fabrication and installation of experimental instrument, the gripper was made as large as a hand size, which further informs the general geometrical dimensions of the PRBM. Specifically, the jaw-length (c) was determined to be 47 mm to enable the experimental measurement of two points. The thickness (t or t_1) of the beam in the R or P joint was adjusted to be 0.8 mm because of the limitation of manufacturing to be discussed in the subsequent section. To reduce the actuation force, the out-of-plane thickness of the gripper is minimized to 5 mm. The double parallelogram with a flexure beam of 12 mm long (L_P) is arranged in the middle, which not only can yield large deformation but also make the gripper compact enough. The gripper was assigned with the material of AL 6082 (EU standard) which is known to have promising mechanical properties like high strength and fatigue limit, where the Young's modulus is E= 69 GPa, Poisson's ratio is δ = 0.33, and yield strength is $[\sigma]$ = 276 MPa.

Table 2: Selected geometrical parameters of the gripper

Symbol	Dim [mm]
R	**3**
r	1
t	0.80
r_1	1
t_1	0.80
L	15

L_P	12
T	4.20
D	15.80
a	55
b	65.50
c	47
d_0	40
d_{10}	75.66
d_{20}	26
e	17.50
f	10

Before manufacturing the prototype, the finite element analysis (FEA) was conducted to obtain its corresponding performances, which were compared with the results of the analytical model. The monolithic gripper adopts Hex Dominant meshing for each rigid bar and subdivides the mesh at the part where the strain concentrates as shown in Fig.4. The simulation was conducted by applying a series of input forces or input displacements. The deformed results show a nearly straight-line parallel jaw trajectory with a negligible parasitic motion. The maximum stress occurs at the flexure hinges as indicated in Fig.5, which increases as the input force/displacement rises. To produce a gripping range of ±1mm of each jaw, the maximum stress generated is 243.2 MPa, which is less than the yield strength 276 MPa. With an input displacement of 0.4 mm, the output displacement of each jaw is about 1.16 mm, which indicates the amplification ratio is about 2.9. The detailed performances (i.e. relationship between input displacement and output displacement and the correlation between input force and output displacement) of the gripper will be studied in Sec .4 with quantitative comparisons among the FEA, analytical and experimental results.

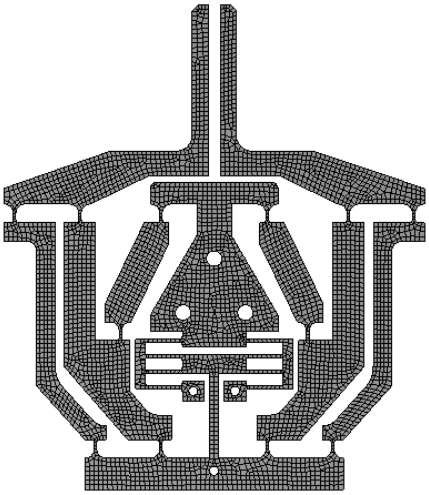

Figure 4 Hex Dominant meshing

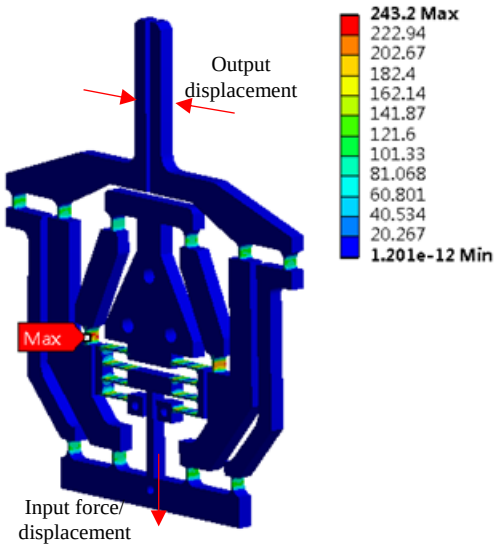

Figure 5 Static analysis

3.2. *Manufacturing and testing*

Computer numerical control (CNC) milling was used to monolithically fabricate the compliant gripper prototype (Fig. 6a) from a piece of AL 6082 plate. Supporting blocks, as shown in Fig. 6b, were first fabricated to ensure the stability of the thin beam as the milling machining produces contact force to the beam.

The experimental set-up includes the compliant gripper, a fixed base, digital gauges (displacement sensors), and an actuator (suspended weights), which is elaborated in Fig. 6c. All the

displacement sensors are produced by Mitutoyo Corporation (Japan) with motion resolution of 1 × 10−3 mm and a negligible spring force between 0.4 N and 0.7 N.

The actuation force is achieved by applying a series of weights on the weight attachment that is connected to the bottom of the gripper through a pulley system. The actuation forces were determined by previous FEA results indicating that the forces less than 140 N will not cause a yield failure. A conservative maximum actuation force of 100 N was set to avoid material's yield, leading to a safety factor of 1.4.

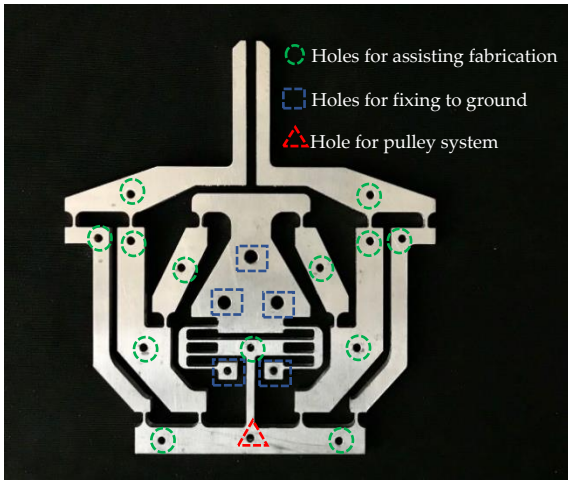

(a) Monolithically fabricated gripper

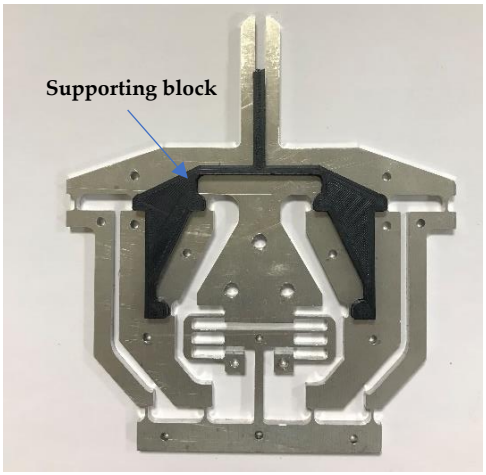

(b) Supporting block used during fabricating

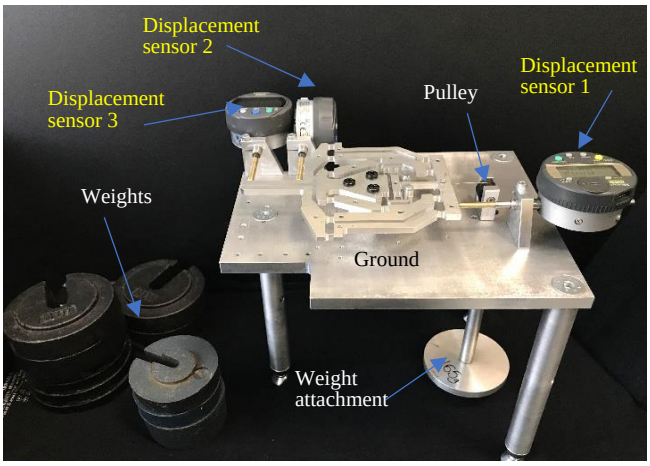

(c) Experimental set-up for the input/output relationship

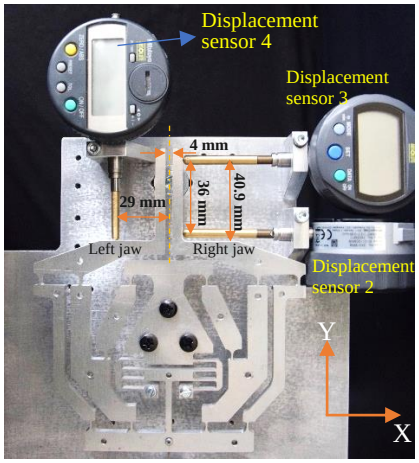

(d) Set-up for testing the jaw performance

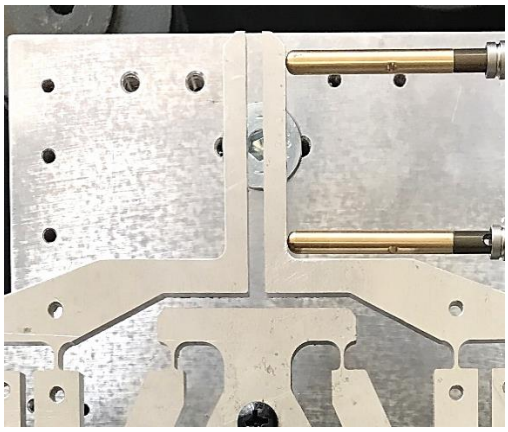

(e) Initial position

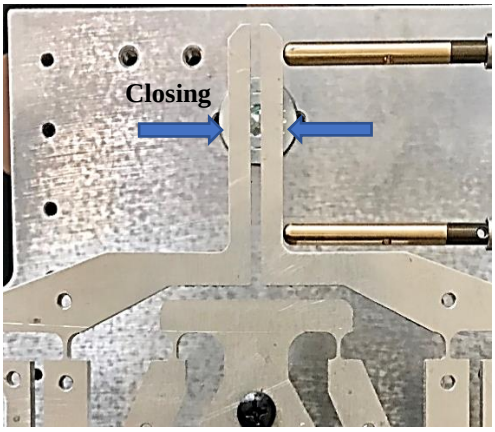

(f) Closure of the jaw

Figure 6 Testing rigs

The actuation/input displacement (Y_{in}) is measured by sensor 1 (Fig. 6(c)). To evaluate the output motions of the jaw, two displacement sensors (sensors 2 and 3 as indicated in Fig. 6(c)) were installed

to collect the primary output translation (X_{out}) and parasitic output rotation (incline angle) of the right jaw. The average between the sensor 2 and sensor 3 measurements is used to denote X_{out}. The difference between the sensor 2 and sensor 3 measurements is used to obtain the incline angle of the jaw since the distance between sensors 2 and 3 is known. The counterclockwise incline angle is defined as positive with regard to the global coordinate system as defined in Fig. 6(d). The jaw's parasitic output translation (displacement in the Y direction) at a specific point is measured by sensor 4 (contacting to the left jaw), as indicated in Fig. 6d. The initial position of the jaw is presented in Fig. 6e. Under a 70 N input, the closing position is shown in Fig. 6f.

Figure 7 shows the flowchart of the experiment procedure. The gripper was actuated by adding 10 N weights until 100 N is reached so that a set of displacements were measured. Each set of displacement measurements were repeated three times to ensure validity. The averaged results of displacement data then were integrated to obtain various correlations characterizing the performances of the gripper.

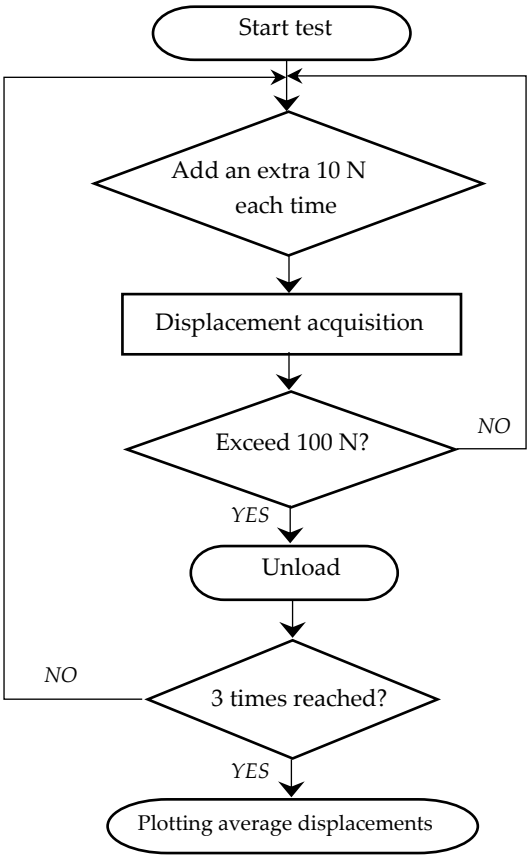

Figure 7 Flowchart of the experiment process

Previous simulation results also suggest that the maximal stress occurs at the flexure hinges in the middle, which is about twice bigger than the other hinges. However, the achievable maximum stress is also related to the manufacturing quality. The experiment shows that the gripper can produce a 0.9 mm motion range for each jaw, which means the gripper can grasp the objects with the diameter between 2.2 mm and 4 mm (gap between two jaws is 4 mm). The gripper can be miniaturized to satisfy different design specifications.

4. Comparisons of results

In this section, the signs of all the forces and displacements are determined based on a new coordinate system as shown in Fig. 6d. Figure 8 compares the jaw's output displacements among three models obtained from the analytical, FEA and experimental results, which increase with the input displacement. The largest deviation can be seen between experimental and FEA results with a

maximum difference of 3.7%. The analytical results are located about between the FEA and experimental results for the second half of the input, which verifies the accuracy of the analytical model. Figure 9 illustrates the comparisons of the relationship between input displacement and input force. The plot suggests an agreement between the analytical and FEA results with only a 1.9% difference. The maximal difference occurs between the experimental and FEA results, which is 4.2%.

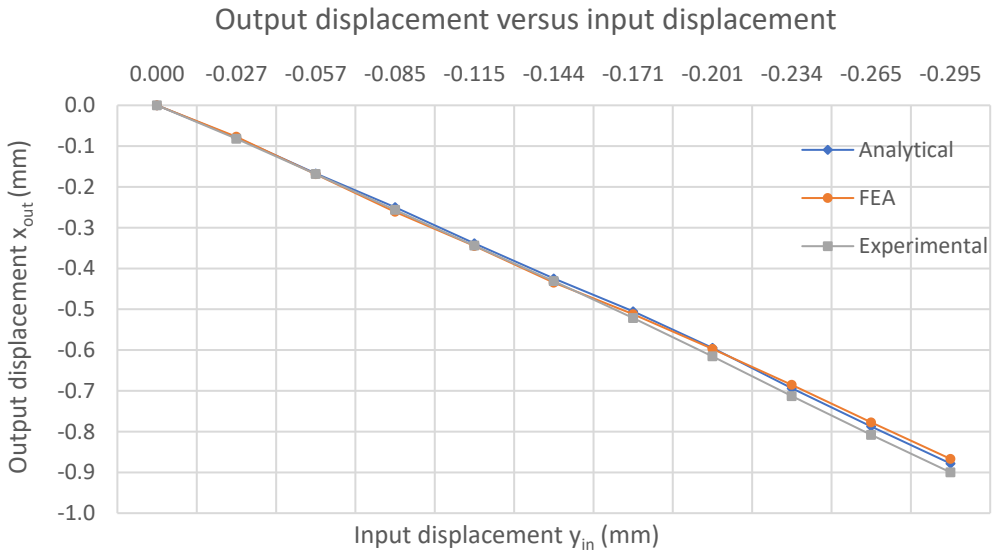

Figure 8 Relationship between output displacement and input displacement

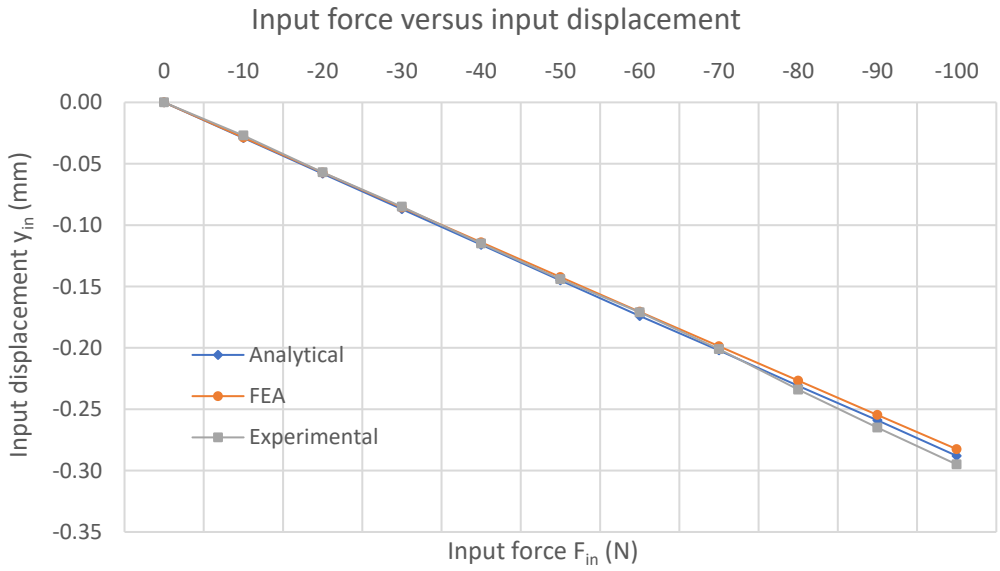

Figure 9 Relationship between input displacement and input force

The investigation on the amplification ratio (output displacement/input displacement) as a function of input displacement is provided in Fig. 10. Equation (5) is used in Fig. 10 to calculate the analytical amplification ratio. The amplification ratio is not ideally a constant value, which increases as the input displacement increases. The analytical and FEA results follow the similar trends under different inputs with a small deviation of 1.7% difference. It is noticeable that the contour of the experimental results fluctuates slightly, which may be due to the relatively low resolution of the displacement sensor. Nevertheless, the overall results show a nearly constant amplification ratio varying from 2.85 to 3.05. To obtain a constant amplification ratio, the design approach proposed in [35] can be referred to.

The parasitic output motions of the jaw are graphically demonstrated in Figs. 11 and 12. In Fig. 11, the FEA results show a steady increase of the incline angle as the input displacement rises and it ends at a maximum value of 2.42×10^{-4} rad, while the experimental results follow the same trend with a small fluctuation. The difference between the FEA and experimental results may be due to the small parasitic displacement that can be not accurately detected by the displacement sensor. Figure 12 illustrates the comparison between the FEA and experimental results for the parasitic Y-direction displacement at the specific point (Fig. 6(d)). The results show a relatively small deviation wherein the FEA results are slightly higher than the experimental results. Since the displacement sensor cannot detect any displacement less than 0.001 mm, the experimental results show a zero parasitic Y-direction displacement under an input displacement of 0.027 mm. The maximum jaw's parasitic Y-direction displacement is 0.01 mm captured by the FEA, which is about 1.1 % of the primary output motion, 0.9 mm, of the jaw (Fig. 8).

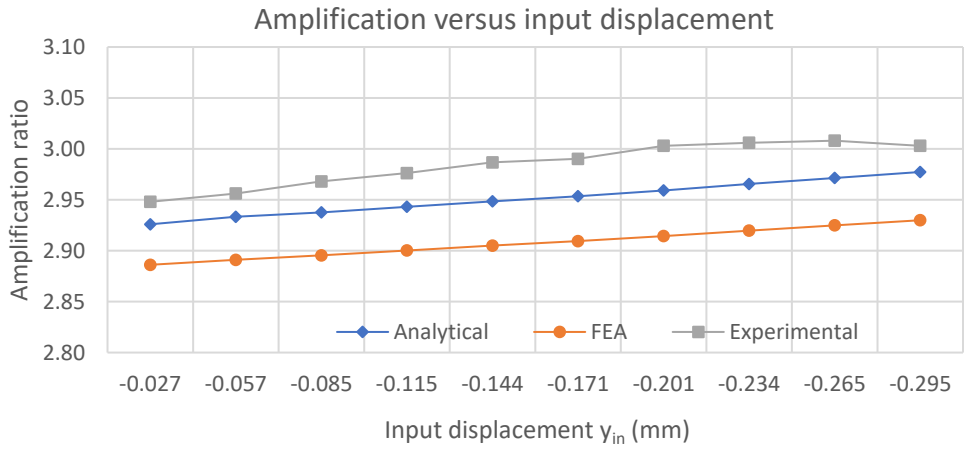

Figure 10 Relationship between amplification ratio and input displacement

Those parasitic output motions lead to non-ideal straight-line parallel jaw trajectory and cannot be captured in the analytical model since they are neglected during the modelling under several assumptions. However, those parasitic motions (small incline angle and Y-direction displacement) do exist in the FEA and experimental models (Figs. 11 and 12), due to several reasons as detailed below. The main reason seems to be the centre drift of the RCCF hinges (R joints) that is identified in FEA or experiment. Generally, the RCCF hinge has better performance than individual corner-filleted rectangular and right-circular flexure hinges considering its integrated flexibility and rotation precision [25], but its larger flexibility slightly scarifies its rotation precision. Nevertheless, there is no ideal R joint in compliant mechanisms in light of the inherent extensible-link kinematic characteristic [19]. The secondary reason is that these links assumed to be rigid in the analytical kinematic model can deform slightly during FEA and experiment, which also contribute to the inaccuracy of the kinematic model.

Under both loading and unloading conditions, the hysteresis testing was performed to further analyze the characteristic of the compliant gripper. The changing patterns for the input displacement and the output displacement are graphically demonstrated in Fig.13. There is no significant hysteresis behavior during lodging and unloading. For the input displacement, the maximum hysteresis error is 5% (9 μm difference), while the maximum hysteresis error for the output displacement is 5.3% (10 μm difference). The hysteresis is mainly due to the bolting connection between the gripper prototype and the ground base.

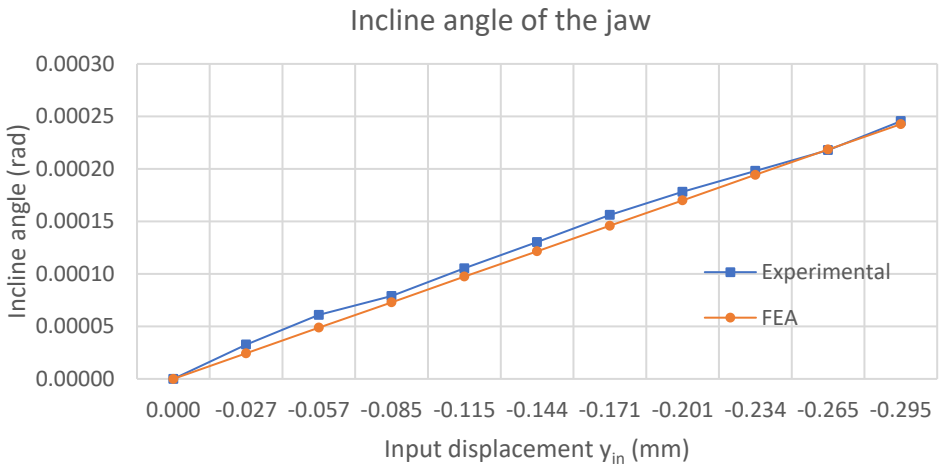

Figure 11 Relationship between jaw incline angle and input displacement

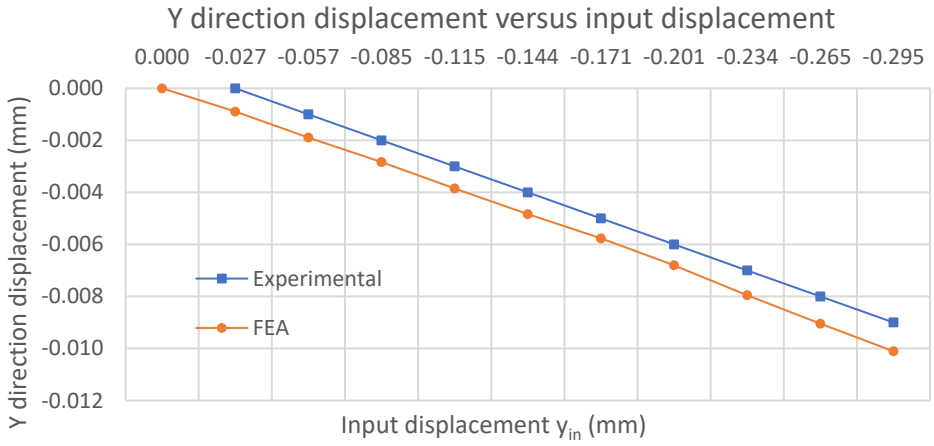

Figure 12 Relationship between Y direction displacement of the jaw and input displacement

5. Conclusions

A systematic development of a compact compliant gripper has been conducted in this paper and its monolithic prototype has been fabricated and tested. This gripper has the ability to generate a nearly straight-line parallel jaw motion in a relatively large stroke, which is dedicated to high precision manipulation in micro-domain. The major characteristics of the gripper is described via a combinatory method including the analytical model and FEA model. Based on the PRBM, a compact Scott-Russell based straight-line mechanism is presented to serve as the kinematic model of the compliant gripper. A parametric model of the compliant gripper has been developed to facilitate the design and optimization, which has been compared with FEA and experimental test results.

The specific performances of the compliant gripper are summarized below:

1) A displacement amplification ratio up to 2.95.
2) A grasping range of 0.9mm of each jaw with a safety factor of 1.4.
3) A nearly straight-line parallel jaw motion.
4) An almost linear relationship between input forces/displacement and output displacement.

Future work will focus on downsizing and non-linear modeling. It is hoped that an advanced actuation system can be employed to improve the manipulation. In addition, the displacement sensors with higher resolution are desired to expedite the measurement accuracy.

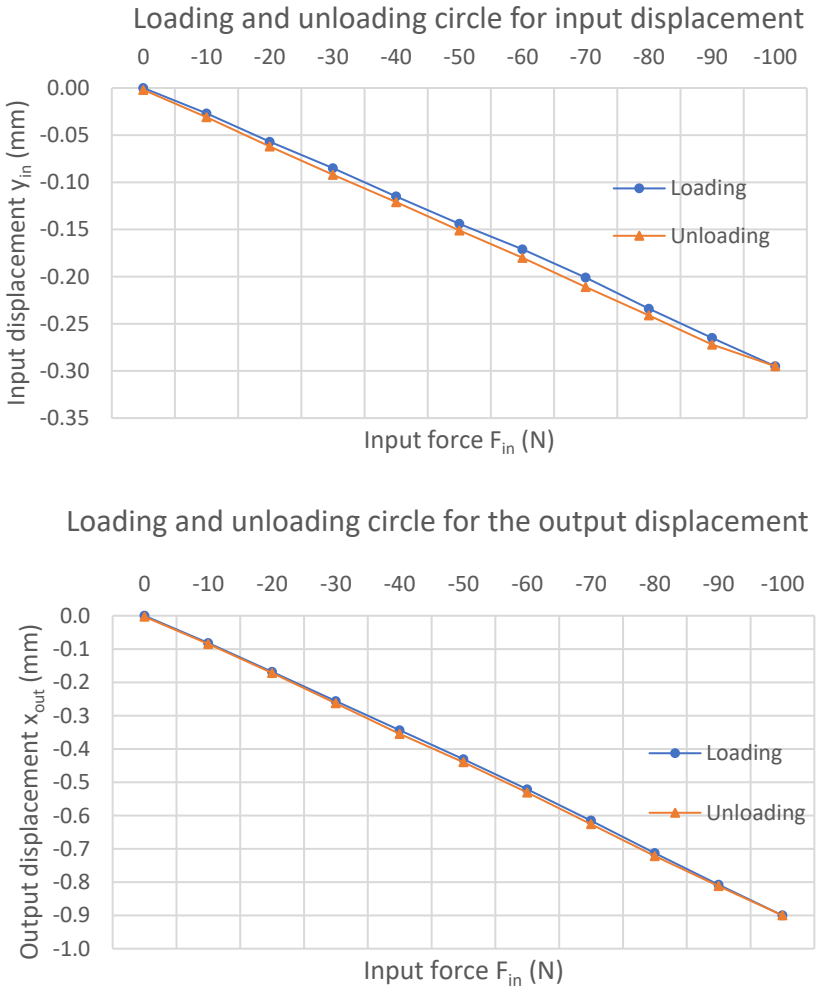

Figure 13 Hysteresis testing

Acknowledgment

The authors would like to thank Mr. Tim Power and Mr. Michael O'Shea in the School of Engineering at University College Cork for their great help in the fabrication work.

References

[1] Howell, Larry L. Compliant mechanisms. John Wiley & Sons, 2001.

[2] Jain, R. K., Majumder, S., Ghosh, B., & Saha, S. (2016). Micro manipulation by a compliant piezoelectric micro gripper towards robotic micro assembly. *International Journal of Mechatronics and Manufacturing Systems*, 9(1), 3-23.

[3] George B, L., & Bharanidaran, R. (2019). Design of compliant gripper for surgical applications. *Australian Journal of Mechanical Engineering*, 1-7.

[4] Zubir, Mohd Nashrul Mohd, Bijan Shirinzadeh, and Yanling Tian. "Development of a novel flexure-based microgripper for high precision micro-object manipulation." *Sensors and Actuators A: Physical* 150.2 (2009): 257-266.

[5] Deaconescu, T., & Deaconescu, A. (2017). Pneumatic Muscle-Actuated Adjustable Compliant Gripper System for Assembly Operations. *Strojniski Vestnik/Journal of Mechanical Engineering*, *63*(4).

[6] Jain, R. K., Majumder, S., & Ghosh, B. (2015). Design and analysis of piezoelectric actuator for micro gripper. *International Journal of Mechanics and Materials in Design*, *11*(3), 253-276.

[7] Bhattacharya, S., Chattaraj, R., Das, M., Patra, A., Bepari, B., & Bhaumik, S. (2015). Simultaneous parametric optimization of IPMC actuator for compliant gripper. *International Journal of Precision Engineering and Manufacturing*, *16*(11), 2289-2297.

[8] Lofroth, M., & Avci, E. (2019). Development of a novel modular compliant gripper for manipulation of micro objects. *Micromachines*, 10(5), 313.

[9] Lamers, A. J., Sánchez, J. A. G., & Herder, J. L. (2015). Design of a statically balanced fully compliant grasper. *Mechanism and machine theory*, 92, 230-239.

[10] Hao, Guangbo, and Ronan Brendan Hand. "Design and static testing of a compact distributed-compliance gripper based on flexure motion." *Archives of Civil and Mechanical Engineering*16.4 (2016): 708-716.

[11] Carrozza, M. C., Menciassi, A., Tiezzi, G., & Dario, P. (1998). The development of a LIGA-microfabricated gripper for micromanipulation tasks. *Journal of Micromechanics and Microengineering*, 8(2), 141.

[12] Jain, R. K., Majumder, S., Ghosh, B., & Saha, S. (2015). Design and manufacturing of mobile micro manipulation system with a compliant piezoelectric actuator based micro gripper. *Journal of Manufacturing Systems*, 35, 76-91.

[13] Mehrabi, H., Hamedi, M., & Aminzahed, I. (2019). A novel design and fabrication of a micro-gripper for manipulation of micro-scale parts actuated by a bending piezoelectric. *Microsystem Technologies*, 1-9.

[14] Sun, Xiantao, et al. "A novel piezo-driven microgripper with a large jaw displacement." *Microsystem Technologies* 21.4 (2015): 931-942.

[15] Wang, D. H., Q. Yang, and H. M. Dong. "A monolithic compliant piezoelectric-driven microgripper: Design, modeling, and testing." *IEEE/ASmE Transactions on mechatronics* 18.1 (2011): 138-147.

[16] Zhang, Dapeng, et al. "Development of a monolithic compliant SPCA-driven micro-gripper." *Mechatronics* 25 (2015): 37-43.

[17] Hao, Guangbo, and Haiyang Li. "Nonlinear analytical modeling and characteristic analysis of a class of compound multibeam parallelogram mechanisms." *Journal of Mechanisms and Robotics* 7.4 (2015): 041016

[18] Beroz, Justin, et al. "Compliant microgripper with parallel straight-line jaw trajectory for nanostructure manipulation." *Proceedings of 26th American Society of Precision Engineering Annual Meeting, Denver, USA*. 2011.

[19] Beroz, J., Awtar, S., & John Hart, A. (2014). Extensible-link kinematic model for characterizing and optimizing compliant mechanism motion. *Journal of Mechanical Design*, 136(3).

[20] Gopal, V., Alphin, M. S., & Bharanidaran, R. (2019). Design of Compliant Mechanism Microgripper Utilizing the Hoekens Straight Line Mechanism. *Journal of Testing and Evaluation*, 49(3).

[21] Ai, W., & Xu, Q. (2014). New structural design of a compliant gripper based on the Scott-Russell mechanism. *International Journal of Advanced Robotic Systems*, 11(12), 192.

[22] Liao, Y. G. (2011). Design and analysis of a modified Scott Russell straight-line mechanism for a robot end-effector. *J Appl Sci Eng Technol*, 4, 42-49.

[23] Xu, Qingsong. "Design and development of a novel compliant gripper with integrated position and grasping/interaction force sensing." *IEEE Transactions on Automation Science and Engineering* 14.3 (2015): 1415-1428.

[24] Nah, S. K., and Z. W. Zhong. "A microgripper using piezoelectric actuation for micro-object manipulation." *Sensors and Actuators A: Physical* 133.1 (2007): 218-224.

[25] Chen, Gui-Min, Jian-Yuan Jia, and Zhi-Wu Li. "Right-circular corner-filleted flexure hinges." *IEEE International Conference on Automation Science and Engineering, 2005.*. IEEE, 2005.

[26] Edwards, Brian T., Brian D. Jensen, and Larry L. Howell. "A pseudo-rigid-body model for initially-curved pinned-pinned segments used in compliant mechanisms." *J. Mech. Des.*123.3 (1999): 464-468.

[27] Joshi, R. S., Mitra, A. C., & Kandharkar, S. R. (2017). Design and analysis of compliant micro-gripper using pseudo rigid body model (PRBM). *Materials Today: Proceedings*, *4*(2), 1701-1707.

[28] Sigmund, Ole. "On the design of compliant mechanisms using topology optimization." *Journal of Structural Mechanics* 25.4 (1997): 493-524.

[29] Bruns, Tyler E., and Daniel A. Tortorelli. "Topology optimization of non-linear elastic structures and compliant mechanisms." *Computer methods in applied mechanics and engineering*190.26-27 (2001): 3443-3459.

[30] Hao, Guangbo, and Ronan Brendan Hand. "Design and static testing of a compact distributed-compliance gripper based on flexure motion." *Archives of Civil and Mechanical Engineering*16.4 (2016): 708-716.

[31] Sun, X., Chen, W., Chen, W., Qi, S., Li, W., Hu, C., & Tao, J. (2019). Design and analysis of a large-range precision micromanipulator. *Smart Materials and Structures*, 28(11), 115031.

[32] Tian, Y., Shirinzadeh, B., Zhang, D., & Alici, G. (2009). Development and dynamic modelling of a flexure-based Scott–Russell mechanism for nano-manipulation. *Mechanical Systems and Signal Processing*, 23(3), 957-978.

[33] Sollpaur, Shrishail B., Maharudra S. Patil, and Suhas P. Deshmukh. "Evaluation of Stiffness and Parametric Modelling of XY Flexure Mechanism for Precision Applications." *Journal of Modeling and Simulation of Materials* 1.1 (2018): 8-15.

[34] Hao, Guangbo, Qiaoling Meng, and Yangmin Li. "Design of large-range XY compliant parallel manipulators based on parasitic motion compensation." *ASME 2013 International Design Engineering Technical Conferences and Computers and Information in Engineering Conference*. American Society of Mechanical Engineers, 2013.

[35] Hao, Guangbo, and Jiaxiang Zhu. "Design of a monolithic double-slider based compliant gripper with large displacement and anti-buckling ability." *Micromachines* 10.10 (2019): 665.